

# Low-Temperature Plasma-Assisted Nanotransfer Printing between Thermoplastic Polymers

By Deuk Yeon Lee, Daniel R. Hines, Christopher M. Stafford, Christopher L. Soles, Eric K. Lin, and Gottlieb S. Oehrlein\*

Much attention has been focused recently on the fabrication of organic-based electronic devices by bottom-up soft lithography, which enables sub-nanoscale patterning at a lower cost and with higher throughput over a larger area than conventional photolithographic techniques. Such nanofabrication tools include inkjet printing, nanoimprint lithography, capillary molding, cold welding, detachment, and transfer printing (TP).<sup>[1–4]</sup> Among soft-lithographic techniques, nano-TP (NTP) has been highlighted because active materials have been easily transferred from a transfer substrate to a flexible-device substrate without using an anisotropic etching process, such as reactive-ion etching, to remove the residual layer in the compressed area. A fabrication process that requires an etch step limits the possible applications of certain soft-lithographic approaches to electronic-device fabrication, because of concerns that active materials can be easily damaged by energetic radiation, ion bombardment, and other interactions. For applications where this process utilizes a thermoplastic polymer material as the device substrate, enhanced adhesion between the printable layer and device substrate has been achieved by thermal cycling, which consists of heating well above the glass-transition temperature ( $T_g$ ) of the polymer(s). However, thermal cycling can lead to dimensional distortion and volume shrinkage of replicated nanostructures when there are sizeable differences in thermal-expansion coefficients between the printable layer and device substrate.<sup>[5,6]</sup> In addition, most low-molecular-weight organic layers used for plastic electronics show bad thermoplastic behavior, and unintended crystallization of the organic layer degrades the device performance of the organic material.<sup>[7]</sup> To overcome these problems, alternative approaches have been investigated, including i) introduction of new stamp materials or resists with low  $T_g$ , such as spin-on glass (SOG), hydrogen silsesquioxane (HSQ), and oligomer compounds;<sup>[7–9]</sup> ii) reducing  $T_g$  to close to room temperature by

modification of the processing atmosphere, including CO<sub>2</sub> absorption and solvent vapor treatment;<sup>[10,11]</sup> and iii) development of nonthermal curing processes, such as step- and flash-imprint lithography, laser-assisted direct imprint, and free-volume contraction.<sup>[12–14]</sup> One main issue is that thermoplastics with low  $T_g$  show low mechanical stability, and that the specific dependency of materials or environments is undesirable for mass production in various applications. This requires a new approach to achieve low-temperature processing in thermal-based soft lithography to compete with UV-based lithographies that exhibit high reproductivity with short tack times.<sup>[15]</sup> Surface modification by techniques such as plasma surface activation, plasma polymerization, and wet-chemical treatment, including self-assembled monolayers (SAMs), have been successfully used in various applications such as adhesion, protective coatings, bioengineering, and nano/microelectronic devices.<sup>[16–19]</sup> Here, plasma surface activation of polymer films will be demonstrated as a way to achieve NTP below the  $T_g$  of two contacting polymers. In TP, one key factor that influences pattern transfer is the differential adhesion strength between the printable layer and the thermoplastic device substrate. Plasma surface activation produces active surface sites on a polymer film by chain scission and ablation.<sup>[20]</sup> These reactive sites are expected to enhance interfacial adhesion and enable TP even below the  $T_g$  of the polymers, which can facilitate dimensional stability of sequential printing steps for the fabrication of multilayer and 3D nanostructures. The use of plasma processes for surface modification also avoids the problems encountered when employing wet-chemical methods, including contamination of surfaces by residual solvent and swelling of the substrate. Another attractive feature of plasma surface activation is its applicability to any substrate, removing the material limitation of interfacial adhesion present in other approaches.

In our previous research, we reported the fabrication of organic and carbon-based thin-film transistors (TFTs) by sequential TP on plastic substrates. The resulting device performance was reported to be comparable to that of organic TFT devices fabricated by more conventional techniques such as vacuum deposition.<sup>[21–23]</sup> However, the processing temperature (up to 170 °C) involved in the TP process limited the registration accuracy of layer-to-layer alignment. The present work demonstrates a lowering of the TP temperature for plasma-treated poly(methyl methacrylate) (PMMA) films printed onto similarly treated poly(ethylene terephthalate) (PET) substrates. In device fabrication, the PMMA film would constitute a dielectric layer that separates source/drain (S/D) electrodes from a gate electrode on a PET substrate.

Figure 1a illustrates the process for TP of an electrode subassembly used in the fabrication of TFT devices on plastic substrates. The TP process is described in detail else-

[\*] Prof. G. S. Oehrlein, D. Y. Lee  
Department of Materials Science and Engineering  
Institute for Research in Electronics and Applied Physics  
University of Maryland College Park, MD 20742 (USA)  
E-mail: oehrlein@umd.edu  
D. R. Hines  
Laboratory for Physical Sciences  
and Department of Physics  
University of Maryland  
College Park, MD 20742 (USA)  
E. K. Lin, C. M. Stafford, C. L. Soles  
Polymers Division  
National Institute of Standards and Technology  
Gaithersburg, MD 20899 (USA)

DOI: 10.1002/adma.200803121

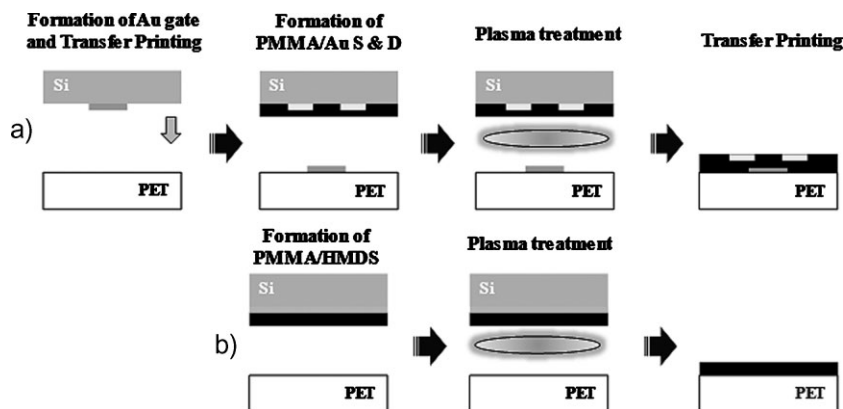


**Figure 1.** Schematic of sequential TP. a) From left to right: formation of Au gate on Si by standard lithography and TP onto PET substrate; formation of Au S/D electrodes on Si followed by spin-coating of PMMA; surface treatment on both surfaces with O<sub>2</sub> and N<sub>2</sub> plasma; TP of PMMA/Au S/D electrodes onto Au-gate-patterned PET. b) Formation of PMMA/HMDS (FDTs) on Si, surface treatment on both sides with O<sub>2</sub> and N<sub>2</sub> plasma, TP of PMMA into PET.

where.<sup>[21,22,24,25]</sup> Briefly, TP involves the transfer of a printable layer from one substrate (transfer substrate) to another (device substrate). The process relies on differential adhesion, where the adhesion of the printable layer to the device substrate is larger than that of the printable layer to the transfer substrate. It has been shown that when the device substrate is a thermoplastic polymer, the necessary differential adhesion can be achieved using pressure and temperature. The TP process, as illustrated in the left panel of Figure 1a, utilizes a PET device substrate, patterned Au features as the printable layer, and a Si transfer substrate. A second sequential print is depicted in the two center panels of Figure 1a. Here, the printable layer is a bilayer composed of patterned Au features and a spin-coated PMMA layer. Prior to the second print step, the polymer surfaces are depicted as being plasma-treated. The resulting electrode subassembly printed onto the PET substrate is illustrated in the right panel of Figure 1a. Typically, our transfer-printed electrode subassemblies have been printed using Au gates 100 nm thick and Au S/D electrodes 30 nm thick, which were fabricated directly onto Si transfer substrates using standard photolithography. The PMMA dielectric layer is shown spin-coated onto the Si transfer substrate containing the patterned Au S/D electrodes. For the experiments presented below and illustrated in Figure 1b, only the polymer film and plastic substrate (no electrodes) are considered. The PET substrates were cut from sheets of Melinex 453/700 with the untreated side used as purchased. The PMMA films were spin-coated onto 1 cm<sup>2</sup> Si substrates using as-purchased MicroChem A7-950K.<sup>[26]</sup> Prior to spin-coating, the Si substrates were cleaned in solvent, treated with UV-ozone for 10 min, and exposed to vapor deposition of hexamethyldisilazane (HMDS) at 150 °C for 10 min. The HMDS SAM reduced the interfacial adhesion between the Si wafer and the PMMA film by lowering the surface energy of the Si wafer.<sup>[27]</sup> Finally, the plasma-treated PMMA films were transfer-printed onto plas-

ma-treated PET substrates at 60, 80, and 100 °C, and 500 psi (3.44 MPa) for 3 min. Before TP, an inductively coupled plasma process employing O<sub>2</sub> and N<sub>2</sub> gas was used for surface treatment on both polymer surfaces.<sup>[28]</sup>

To investigate the change in surface chemistry with plasma treatment, X-ray photoelectron spectroscopy (XPS) was performed. Since the measurements were single-point, standard uncertainties were not determined from them. The O/C and N/C ratios obtained from deconvolution of the C 1s, O 1s, and N 1s spectra are shown in Figure 2 as functions of plasma chemistry. More details on the XPS spectra will be presented in a future publication.<sup>[29]</sup> For PMMA, O<sub>2</sub>-plasma treatment mainly breaks the C–H and C–O bonds in ether groups to form O-containing functional groups such as alcohol and carbonyl groups, while in N<sub>2</sub> plasma carbonyl and amide groups

(O=C–NH–) are generated. The O/C ratio increases from 0.38 (untreated) to 0.47 in O<sub>2</sub> plasma. After N<sub>2</sub>-plasma treatment, the O/C ratio decreases to 0.25, while the N/C ratio increases to 0.34, which indicates that a large amount of oxygen is replaced by nitrogen. For PET, after O<sub>2</sub>-plasma treatment, chain scission of the C–C bond in the backbone and hydrogen abstraction generates alcohol and carbonyl groups. As a result, the O/C ratio dramatically increases from 0.36 (untreated) to 0.53. In N<sub>2</sub> plasma, carbonyl, amide, and amine groups (>C–N<) are generated at dangling bonds in aromatic ring structures. The O/C ratio decreases slightly from 0.36 to 0.28, and the N/C ratio is 0.3. Nitrogen concentration is only detected in samples treated with N<sub>2</sub> plasma. A higher N/C ratio is obtained in PMMA (0.34) than in PET (0.30), which is attributed to the high etching resistance of PET caused by its aromatic-ring structure.<sup>[30]</sup>

The surface energies of plasma-treated PET and PMMA are shown in Figure 3, and were calculated from contact-angle measurements employing deionized water, formamide, and diiodomethane as probe fluids. All samples exhibited contact angles within ±2° of the average value reported herein, and this is taken as the standard uncertainty of the measurement. It is well known that incorporation of oxygen and nitrogen with high surface polarity at polymer surfaces increases the surface

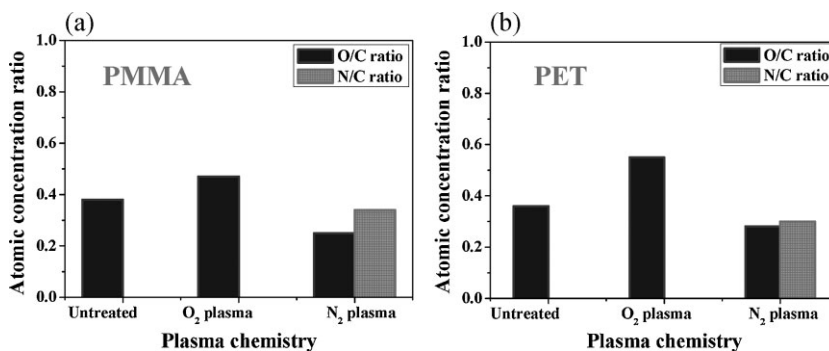


**Figure 2.** Variation of the O/C and N/C ratios for a) PMMA and b) PET calculated from deconvolution of the XPS spectra after plasma treatment.

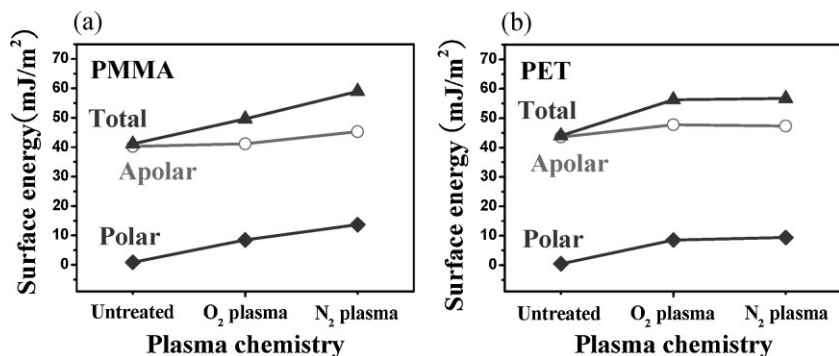


**Figure 3.** Change of total surface energy (▲) (including polar (◆) and apolar (○) components) as a function of plasma chemistry for a) PMMA and b) PET.

energy.<sup>[31]</sup> This very trend can be observed in this data. Surface-energy variation is more evident in the polar component of the surface energy than in the apolar (dispersion) component. Comparing O<sub>2</sub> with N<sub>2</sub> plasma, the surface energy is higher in the N<sub>2</sub> than in the O<sub>2</sub> plasma for PMMA, while it is unchanged in the case of PET. Because PMMA and PET contain oxygen functional groups in their basic structures, new generation of nitrogen-related groups by N<sub>2</sub>-plasma treatment can cause the polymer surface to become more hydrophilic. The lower nitrogen incorporation in PET compared to PMMA may be related to the presence of inactive aromatic rings in PET, which reduce the number of potential reaction sites and help to stabilize the free radicals created from ester-bond cleavage and H abstraction through electronic resonance.<sup>[30]</sup>

Figure 4 illustrates the proposed routes for incorporating functionalities on the polymer surfaces after O<sub>2</sub>- and N<sub>2</sub>-plasma

treatment. The plasma treatment will introduce disorder in the polymer surface region, which is not accounted for in the model of Figure 4. The carbon skeleton of PMMA consists of a saturated C–C backbone with dangling ester groups. Possible bond-breaking sites in PMMA by plasma are shown in Figure 4a.<sup>[32]</sup> New functional groups can be grafted into the polymer structure through chain scission of ester groups, resulting in carboxyl (Fig. 4a, part b) and carbonyl groups (Fig. 4a, part i). Dangling bonds in the backbone and chain scission of the C–H bond in methyl groups also generate oxygen-related functional groups (Fig. 4a, part a,c). Regarding N<sub>2</sub> plasma, nitrogen atoms preferentially attach to oxygen-bonded carbon sites (Fig. 4a, parts e,f), leading to the formation of amide structures (O=C–NH–).<sup>[33]</sup> Compared with PMMA, PET has an additional phenyl-ring structure as shown in Figure 4b. Dangling bonds (Fig. 4a, ①) attained through hydrogen abstraction from phenyl rings and the C–C bonds in the backbone (–CH<sub>2</sub>–CH<sub>2</sub>–; Fig. 4a, ②) with a little portion of methylene carbons singly bound to oxygen (C–O–C; Fig. 4a, ③) in ether groups are the main sites for chain scission. As well as generation of carboxyl (Fig. 4a, part b) and carbonyl (Fig. 4a, part i) groups, the hydrogen atoms that are bound to the benzene ring should be substituted by hydroxyls (Fig. 4a, part g). After N<sub>2</sub>-plasma treatment on PET, in addition to amide groups (Fig. 4a, part e), amine groups (>C–N<) can be generated at dangling-bond sites in the aromatic-ring structures (Fig. 4a, part j).<sup>[34]</sup> Therefore, rearrangement of existing ester (hydroxyl) and ether groups modified by O<sub>2</sub> plasma and new amine and amide groups introduced by N<sub>2</sub> plasma, including dangling-related reactive sites such as carbonyl (C=O), carboxyl (COOH), and hydroxyl (–OH), are the main functionalities generated on the surfaces of both polymers.

The influence of these reactive functional groups induced by plasma treatment on the adhesion behavior between the two polymers is qualitatively illustrated in Figure 5. Here, the results of TP-untreated and plasma-treated PMMA films on untreated and plasma-treated PET substrates are shown for printing temperatures of 60, 80, and 100 °C at 500 psi (3.44 MPa) for 3 min. For this qualitative evaluation of adhesion, the TP efficiency (TPE) was defined as the percentage area of PMMA film successfully transferred onto the PET substrate. Accompanying the graphs (Fig. 5a–c) are optical images of the Si transfer substrate after TP (Fig. 5d), in which the TPE was 95% (almost no PMMA residual was left on the transfer substrate), 67% (about half the PMMA did not transfer to the PET), and 5% (where the PMMA basically did not print). As shown in Figure 5a–c, the TPE strongly depends on the processing temperature and plasma chemistry. As the processing tempera-

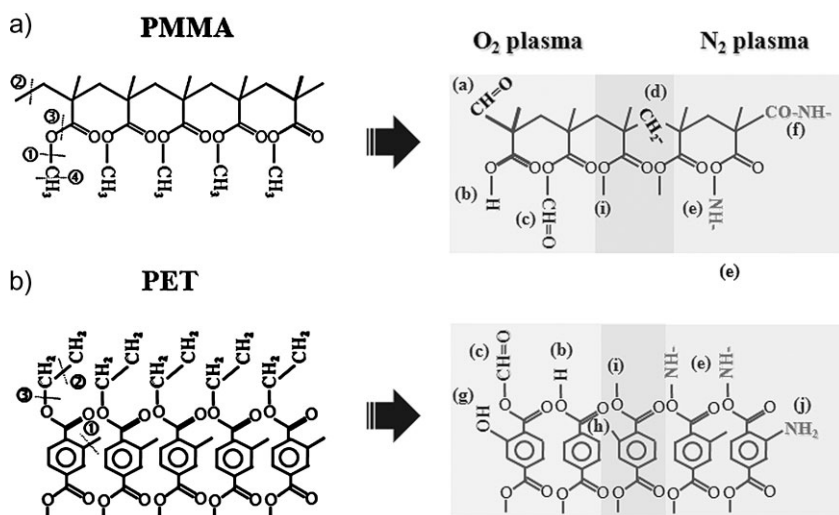


**Figure 4.** Schematic of surface functionalities before and after surface treatment with O<sub>2</sub> and N<sub>2</sub> plasma for a) PMMA and b) PET. Rearrangement of existing ester (hydroxyl) and ether groups modified by O<sub>2</sub> plasma and new amine and amide groups introduced by N<sub>2</sub> plasma including dangling reactive sites (overlap area) are the main functionalities generated on the surfaces of both polymers. ①: Methylene carbons singly bound to oxygen (C–O–C) in ether groups; ②: C–C bonds in backbone (–CH<sub>2</sub>–CH<sub>2</sub>–); ③: carbon atoms of the carboxylic groups (O–C=O); ④: C–H bonds in methyl groups (–CH<sub>3</sub>).

ture decreases, the number of successful printing conditions also decreases, whereas when both surfaces are treated, better transferability is exhibited than when only one polymer surface is treated. For the lowest printing temperature studied (60 °C), O<sub>2</sub>-plasma-treated PMMA/O<sub>2</sub>-plasma-treated PET (O<sub>2</sub>-PMMA/O<sub>2</sub>-PET) and N<sub>2</sub>-plasma-treated PMMA/O<sub>2</sub>-plasma-treated PET (N<sub>2</sub>-PMMA/O<sub>2</sub>-PET) were the only two printing combinations that resulted in a nonzero TPE. Interestingly, the TPE of O<sub>2</sub>-PMMA/N<sub>2</sub>-PET at 60 °C was zero, which means the effect of plasma treatment on adhesion is dependent on the initial polymer structure.

Based on TPE data between blanket samples, the relationship between transferability, processing temperature, and plasma surface activation was determined. Without plasma treatment, the only printable temperature was over 170 °C, well above the *T<sub>g</sub>*s of PMMA (105 °C) and PET (75 °C), revealing that without plasma treatment, a high processing temperature is needed for pattern transfer. In the case of plasma treatment of only one surface, the printing temperature was reduced to 100 °C, which is near the *T<sub>g</sub>* of PMMA and above that of PET. Plasma treatment of both surfaces can further decrease the printing temperature to 60 °C, below the *T<sub>g</sub>* of both polymers. The *T<sub>g</sub>*-dependent transferability is related to the dynamics of polymer chains. When the processing temperature is increased with an applied pressure, the chain ends of the two thermoplastic polymers can start crossing the interface, resulting in rearrangement or restructuring of surface molecular groups. Well above *T<sub>g</sub>*, the surface changes from a glassy to a viscoelastic state, which

enhances its interfacial adhesion.<sup>[35]</sup> In the case of plasma-treated polymers, comparable adhesion can be obtained even below *T<sub>g</sub>* by increasing the number of polar functional groups at the interface rather than interdiffusion of chains. Therefore, hydrophilic surfaces modified via plasma treatment are reactive enough to generate the critical interfacial adhesion necessary to promote film transfer, enabling printing below the *T<sub>g</sub>* of both polymers. Adhesion at lower temperatures is facilitated in part by stronger intermolecular forces, such as hydrogen bonds, acid–base interactions, or covalent bonds, which are a direct consequence of the plasma-modification process.<sup>[36]</sup>

In order to obtain further insight into the quantitative analysis of interfacial adhesion, the interfacial work of adhesion was calculated based on “harmonic” mean and force addition.<sup>[37,38]</sup> The work of adhesion, *W*<sub>12</sub>, between materials 1 and 2 can be estimated from

$$W_{12} = \gamma_1(1 + \cos \theta) \\ = 4(\gamma_1^d + \gamma_2^d/\gamma_1^d + \gamma_2^d) + 4(\gamma_1^p + \gamma_2^p/\gamma_1^p + \gamma_2^p) \quad (1)$$

where  $\theta$  is the contact angle measured and the superscripts *d* and *p* refer to the dispersion and polar components, respectively, of the interfacial surface energy ( $\gamma_{12}$ ). This equation is applicable to low-energy systems, such as organic liquids, water, polymers, and organic pigments. Although Equation 1 reflects the thermodynamic work of adhesion, this is the lower limit, simply based on surface energetics. The actual work of adhesion will be much

higher, as a result of chain entanglement, diffusion, and roughness. Table 1 shows the work of adhesion between untreated and plasma-treated PMMA and untreated and plasma-treated PET using the surface energy evaluated from Figure 3. The results show clear differences between combinations of plasma-treated and untreated surfaces, and appear to be consistent with the general trends in TPE presented in Figure 5. However, differences between adhesion behavior calculated from wettability (Equation 1) and our experiments are evident, and may be attributable to strain-induced temperature effects and/or kinetic effects associated with the experimental results, such as peeling speed, applied force, and the time interval associated with the manual demolding process.<sup>[39]</sup> Indeed, under certain printing conditions, it has been observed visually that printing results were better at lower temperatures, presumably as a result of less thermal strain from differential thermal contraction upon sample cooling. The details associated with the differences between Figure 5 and Table 1 will be the subject of future work, which will include a quantitative experimental measurement of the work of adhesion using an edge-lift-off adhesion test.

To demonstrate the concept further, it is desirable to incorporate plasma treatment into the fabrication of complete electrode subas-

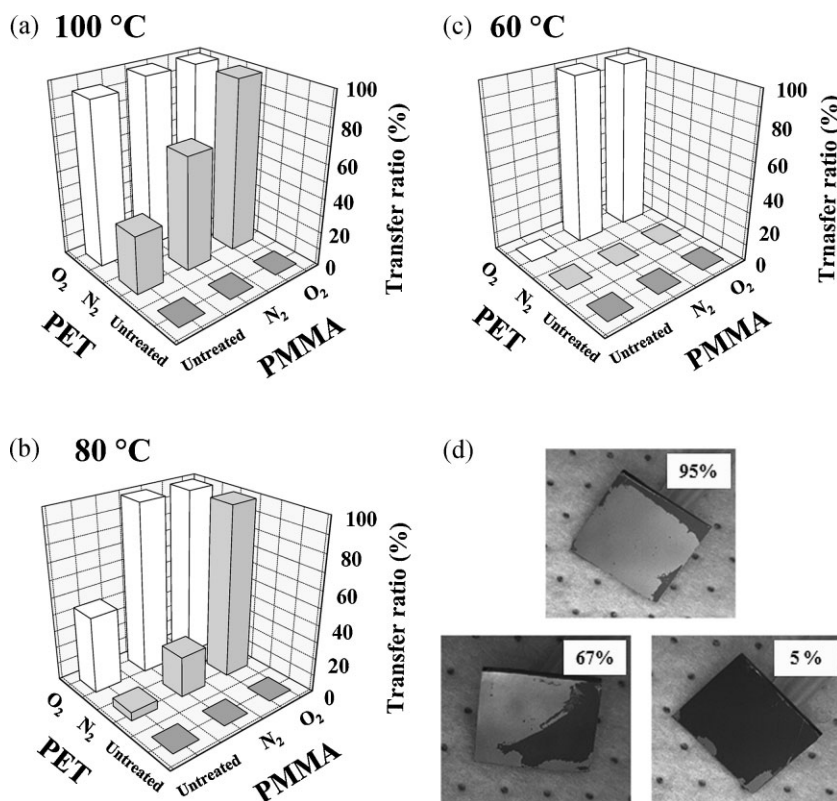


**Figure 5.** TPE as a function of plasma chemistry at a) 100, b) 80, and c) 60 °C. d) Optical images of Si transfer substrate after TP.

**Table 1.** Interfacial work of adhesion calculated using harmonic mean and force addition as functions of plasma chemistry and processing temperature.

Interfacial work of adhesion [m] m <sup>-2</sup>		PMMA		
		O <sub>2</sub> -treated	N <sub>2</sub> -treated	Untreated
PET	O <sub>2</sub> -treated	105.4	114.0	90.5
	N <sub>2</sub> -treated	105.8	114.8	90.2
	Untreated	86.4	90.6	84.9

semblies on plastic substrates (as illustrated in Fig. 1a). This is shown schematically in Figure 6a. The lower left panel represents a 100 nm thick, 200 μm wide Au gate electrode (“+” sign) that was previously transfer-printed onto a PET device substrate. The upper-left panel represents a PMMA film spin-coated over 30 nm thick by 100 μm wide Au S/D electrodes (four sets of two L-shaped patterns separated by a gap) previously patterned on a Si transfer substrate. The lower-right panel represents the printed electrode subassembly on a PET substrate with the gate and S/D electrodes separated by a PMMA dielectric layer. Printing of electrode subassemblies requires, additionally, that the adhesion at the PMMA/PET interface not only be greater than the adhesion at the PMMA/Si interface, but also greater than the adhesion at the Au/Si interface. As seen by comparing the printing conditions with (Fig. 6) and without (Fig. 5) the Au electrodes, a slightly higher printing temperature is needed to overcome the adhesion at the Au/Si interface, indicating that the Au/Si interface has a higher adhesion than the PMMA/Si interface. The results of fabricating electrode subassemblies where the polymer surfaces were plasma-treated prior to TP are tabulated in Figure 6b. The optical image on the left illustrates unsuccessful printing of untreated PMMA onto untreated PET at 80 °C. The PMMA and Au S/D electrodes bilayer was not successfully printed at this temperature. In fact, for untreated PMMA and untreated PET,

printing was not observed below 140 °C. In contrast, with plasma surface activation, fully printed electrode subassemblies could be fabricated at temperatures as low as 80 °C, as shown in the middle and right panels of Figure 6b for plasma treatment of O<sub>2</sub>-PMMA/O<sub>2</sub>-PET and N<sub>2</sub>-PMMA/O<sub>2</sub>-PET, respectively. Considering that the T<sub>g</sub> of PET and PMMA is 75 and 105 °C, respectively, we have found that plasma surface activation allows for TP of a 3D pattern near or even below the T<sub>g</sub> of both polymers.

To conclude, it has been demonstrated that plasma activation of PMMA and PET surfaces can enable transfer printing at dramatically lower processing temperatures. Polar functional groups introduced by plasma surface activation render the polymer surfaces more hydrophilic and cause a dramatic increase in the interfacial adhesion. This enables lowering of the substrate temperature at which NTP can be successfully performed from 170 to 60 °C. The observed changes in transferability between the two polymers with plasma chemistry and processing temperature are consistent with the observed trends in the work of adhesion as a result of plasma surface activation. Lowering the temperature at which successful NTP processes can be performed to below the T<sub>g</sub> of each component by plasma surface activation is a promising method to facilitate industrial implementation of soft lithographies involving thermoplastic polymer materials.

### Experimental

**Plasma Surface Activation:** An inductively coupled plasma was used for surface treatment of PET and PMMA with O<sub>2</sub> or N<sub>2</sub> gas at 10 mTorr using 300 W of radio-frequency (rf) power for 15 s [28]. The substrate was located at the center of the sample holder that was cooled by the circulation of a cooling liquid to 15 °C to prevent sample heating. The total gas flow into the reactor was set at 20 standard cubic centimeters per minute (sccm). Before each experiment, the chamber was cleaned using O<sub>2</sub> plasma, followed by a 3 min chamber seasoning at the conditions for the next experiment.

**Transfer Printing:** TP was performed using a NANONEX 2500 imprint machine at 500 psi (3.44 MPa) for 3 min at various processing temperatures. Both the 100 nm thick Au gate and the 30 nm thick Au S/D electrodes were fabricated directly on Si transfer substrates using standard photolithography. The electrodes/substrate were first exposed to mercaptobenzene thiol for 2 h in a custom-made vapor-deposition chamber and then exposed to the release layer molecule (tridecafluoro-1,1,1,2,2-tetrahydrooctyl) trichlorosilane (FDTs) for 2 min in a second vapor-deposition chamber. After each SAM treatment, the electrodes/substrate were rinsed in 2-propanol and at the end stored in a dry nitrogen purge box. PMMA was used as purchased from Microchem with a molar mass of 950 000 g mol<sup>-1</sup> and a concentration of 7% by mass in anisole (A7). Typically, the PMMA was spin-coated at 2500 rpm (262 rad s<sup>-1</sup>) and baked on a hot plate at 90 °C for 3 min. The resulting dielectric film was approximately 600 nm thick.

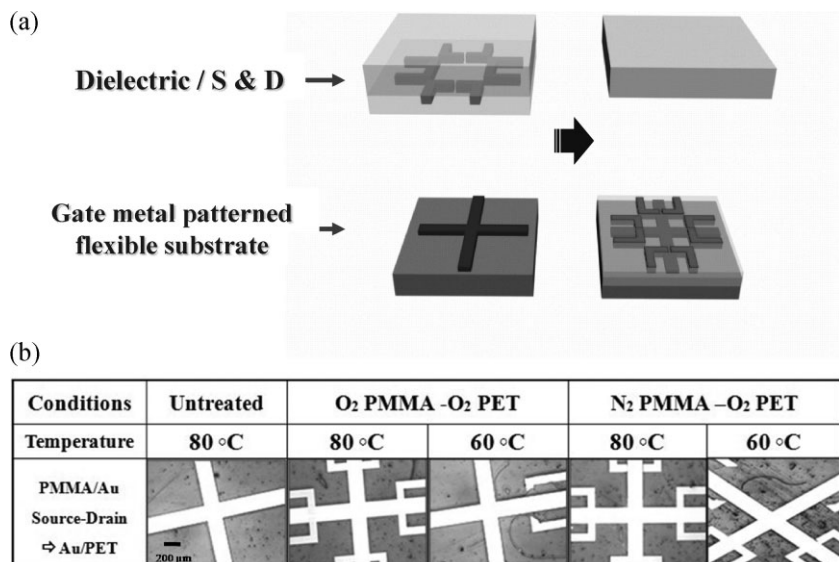


**Figure 6.** a) Schematic diagram of plasma-treated 3D pattern transfer (electrode subassembly) and b) optical images of 3D patterns after transfer printing as a function of plasma treatments and printing temperature.

### Acknowledgements

Official contribution of the National Institute of Standards and Technology; not subject to copyright in the United States. We gratefully acknowledge support of this work from NIST, NASA, and LPS. This work was also supported in part by the Center for

Nanomanufacturing and Metrology at the University of Maryland. In addition, this work was partially supported by the Korea Research Foundation Grant funded by the Korean Government (MOEHRD, Basic Research Promotion Fund) (KRF-J03003).

Received: October 23, 2008

Revised: January 9, 2009

Published online: March 26, 2009

- [1] E. Menard, M. A. Meitl, Y. Sun, J.-U. Park, D. J.-L. Shir, Y.-S. Nam, S. Jeon, J. A. Rogers, *Chem. Rev.* **2007**, *107*, 1117.
- [2] C. Kim, P. E. Burrows, S. R. Forrest, *Science* **2000**, *288*, 831.
- [3] J. H. Choi, D. Kim, P. J. Yoo, H. H. Lee, *Adv. Mater.* **2005**, *17*, 166.
- [4] Y.-L. Loo, R. L. Willett, K. W. Baldwin, J. A. Rogers, *J. Am. Chem. Soc.* **2002**, *124*, 7654.
- [5] Y. Ding, H. W. Ro, J. F. Douglas, R. L. Jones, D. R. Hines, A. Karim, C. L. Soles, *Adv. Mater.* **2007**, *19*, 1377.
- [6] D.-Y. Khang, H. Yoon, H. H. Lee, *Adv. Mater.* **2001**, *13*, 749.
- [7] D. Pisignano, L. Persano, M. F. Raganato, P. Visconti, R. Cingolani, G. Barbarella, L. Favaretto, G. Gigli, *Adv. Mater.* **2004**, *16*, 525.
- [8] S. Matsui, Y. Igaku, H. Ishigaki, J. Fujita, M. Ishida, Y. Ochiai, H. Namatsu, M. Komuro, *J. Vac. Sci. Technol. B* **2003**, *21*, 688.
- [9] W. M. Choi, M. Y. Song, O. O. Park, *Microelectron. Eng.* **2006**, *83*, 1957.
- [10] H. Schmid, B. Michel, *Macromolecules* **2000**, *33*, 3042.
- [11] D. Y. Khang, H. H. Lee, *Appl. Phys. Lett.* **2000**, *76*, 870.
- [12] T. Bailey, B. J. Choi, M. Colburn, M. Meissl, S. Shaya, J. G. Ekerdt, S. V. Sreenivasan, C. G. Willson, *J. Vac. Sci. Technol. B* **2000**, *18*, 3572.
- [13] S. Y. Chou, C. Keimel, J. Gu, *Nature* **2002**, *417*, 835.
- [14] D. Y. Khang, H. Yoon, H. H. Lee, *Adv. Mater.* **2001**, *13*, 749.
- [15] S.-J. Choi, P. J. Yoo, S. J. Baek, T. W. Kim, H. H. Lee, *J. Am. Chem. Soc.* **2004**, *126*, 7744.
- [16] N. Patrino, C. Mccague, P. R. Norton, N. O. Petersen, *Langmuir* **2007**, *23*, 715.
- [17] K. E. Schmalenberg, H. M. Buettner, K. E. Urich, *Biomaterials* **2004**, *25*, 1851.
- [18] J. S. Kim, R. H. Friend, F. Cacialli, *J. Appl. Phys.* **1999**, *86*, 2774.
- [19] R. K. Smith, P. A. Lewis, P. S. Weiss, *Prog. Surf. Sci.* **2004**, *75*, 1.
- [20] J. H. O'Donnell, *ACS Symp. Ser.* **1991**, *475*, 402.
- [21] D. R. Hines, V. W. Ballarotto, E. D. Williams, Y. Shao, S. A. Solin, *J. Appl. Phys.* **2007**, *101*, 024503.
- [22] D. R. Hines, S. Mezheny, M. Breban, E. D. Williams, V. W. Ballarotto, G. Esen, A. Southard, M. S. Fuhrer, *Appl. Phys. Lett.* **2005**, *86*, 163101.
- [23] J. H. Chen, M. Ishigami, C. Jang, D. R. Hines, M. S. Fuhrer, E. D. Williams, *Adv. Mater.* **2007**, *19*, 3623.
- [24] D. R. Hines, A. Southard, M. S. Fuhrer, *J. Appl. Phys.* **2008**, *104*, 024510.
- [25] D. R. Hines, A. E. Southard, A. Tunnell, V. Sangwan, T. Moore, J.-H. Chen, M. S. Fuhrer, E. D. Williams, *Proc. SPIE* **2007**, 66580Y.
- [26] Certain equipment, instruments, and materials are identified in this paper in order to adequately specify the experimental details. Such identification does not imply recommendation by the National Institute of Standards and Technology nor does it imply the materials are necessarily the best available for the purpose.
- [27] S. C. Lim, S. H. Kim, J. H. Lee, M. K. Kim, D. J. Kim, T. Zyung, *Synth. Met.* **2005**, *148*, 5.
- [28] X. Li, L. Ling, X. Hua, M. Fukasawa, G. S. Oehrlein, *J. Vac. Sci. Technol. A* **2003**, *21*, 284.
- [29] D. Y. Lee, D. R. Hines, C. M. Stafford, C. L. Soles, E. K. Lin, unpublished.
- [30] P. Groning, M. Collaud, G. Dieter, L. Schlapbach, *Vide Couches Minces* **1994**, *272*, 140.
- [31] H. Lim, Y. Lee, S. Han, J. Cho, K. J. Kim, *J. Vac. Sci. Technol. A* **2001**, *19*, 1490.
- [32] H. Yasuda, *Plasma Polymerization*, Academic Press, New York **1988**.
- [33] M. K. Shi, G. Dunham, M. E. Gross, G. L. Graff, P. M. Martin, *J. Adhes. Sci. Technol.* **2000**, *14*, 1485.
- [34] C. Riccardi, R. Barni, E. Selli, G. Mazzone, M. R. Massafra, B. Marcandalli, G. Poletti, *Appl. Surf. Sci.* **2003**, *211*, 386.
- [35] N. Maeda, N. Chen, M. Tirrell, J. N. Israelachvili, *Science* **2002**, *297*, 379.
- [36] I. S. Lee, R. P. Wool, *J. Adhes.* **2001**, *75*, 299.
- [37] A. W. Adamson, A. P. Gast, *Physical Chemistry of Surfaces*, Wiley, New York **1997**, Ch. 4.
- [38] S. Y. Park, T. G. Kwon, H. H. Lee, *Adv. Mater.* **2006**, *18*, 1861.
- [39] M. A. Meitl, Z.-T. Zhu, V. Kumar, K. J. Lee, X. Feng, Y. Y. Huang, I. Adesida, R. G. Nuzzo, J. A. Rogers, *Nat. Mater.* **2006**, *5*, 33.